


## Article

# Computational Screening and Experimental Validation on Multicomponent Crystals of a New Class of Janus Kinase (JAK) Inhibitor Drug with Improved Solubility

Yujiang Xie <sup>1,2,†</sup>, Genpei Shi <sup>1,2,†</sup>, Jie Sun <sup>1,2</sup>, Si Li <sup>1,2</sup>, Wei Gao <sup>3,\*</sup>, Yimin Hu <sup>3</sup>, Chang Zu <sup>3</sup>, Weiwei Tang <sup>1,2,\*</sup>  and Junbo Gong <sup>1,2</sup>

<sup>1</sup> School of Chemical Engineering and Technology, State Key Laboratory of Chemical Engineering, The Co-Innovation Center of Chemistry and Chemical Engineering of Tianjin, Tianjin University, Tianjin 300072, China

<sup>2</sup> Haihe Laboratory of Sustainable Chemical Transformations, Tianjin 300192, China

<sup>3</sup> Jiangsu Hengrui Pharmaceuticals Co., Ltd., Lianyungang 222000, China

\* Correspondence: gaoweipharma@163.com (W.G.); wwtang@tju.edu.cn (W.T.); Tel.: +86-22-27405754 (W.T.); Fax: +86-22-27374971 (W.T.)

† These authors contribute equally to this work.

**Abstract:** Developing multicomponent crystal forms, especially cocrystals and salts, is becoming a promising pathway to improve the solubility and bioavailability of drugs. Herein, new multicomponent crystals of SHR0302, a new generation of Janus Kinase (JAK) inhibitor that suffers from poor solubility, were developed based on a cooperative approach of computational and experimental coformer screenings. Virtual screening methods, including the conductor-like screening model for realistic solvents (COSMO-RS) and molecular complementary (MC) analysis, were employed to predict the binding affinity between SHR0302 and selected cofomers. The developed screening method was capable of reducing the screening database to 30 cofomers from a total of 42 proposed cofomers. The proof-of-concept experimental screening study was performed to demonstrate the efficiency of computational screening, wherein three new multicomponent crystalline forms were found and fully characterized by powder X-ray diffraction, thermal analysis, and IR and <sup>1</sup>H-NMR spectroscopy. Further, the measurements of the solubility property of these new multicomponent crystal forms reveal an apparent promotion compared with the drug alone. Finally, the receiver operator characteristic (ROC) curve was used to assess the prediction performance of the COSMO-RS model. It was found that the established screening model can effectively shorten the experimental screening time and efforts.

**Keywords:** multicomponent crystals; cocrystals; COSMO-RS; cocrystal prediction; solubility enhancement



**Citation:** Xie, Y.; Shi, G.; Sun, J.; Li, S.; Gao, W.; Hu, Y.; Zu, C.; Tang, W.; Gong, J. Computational Screening and Experimental Validation on Multicomponent Crystals of a New Class of Janus Kinase (JAK) Inhibitor Drug with Improved Solubility. *Crystals* **2022**, *12*, 1722. <https://doi.org/10.3390/cryst12121722>

Academic Editor: Petros Koutsoukos

Received: 13 October 2022

Accepted: 24 November 2022

Published: 27 November 2022

**Publisher's Note:** MDPI stays neutral with regard to jurisdictional claims in published maps and institutional affiliations.



**Copyright:** © 2022 by the authors. Licensee MDPI, Basel, Switzerland. This article is an open access article distributed under the terms and conditions of the Creative Commons Attribution (CC BY) license (<https://creativecommons.org/licenses/by/4.0/>).

## 1. Introduction

Multicomponent crystalline forms such as cocrystals and salts are an integral part of the crystalline-phase landscape of an active pharmaceutical ingredient (API). They represent the combination of API molecules with other physiologically acceptable acids, alkalis, and non-ionic compound molecules in the same lattice by hydrogen bond,  $\pi$ - $\pi$  stacking, *van der Waals* force, and other non-covalent bonds [1,2]. Creating Multicomponent crystalline forms has been recognized as one of the effective approaches for modifying the physicochemical properties of active pharmaceutical ingredients (APIs), such as solubility, stability, dissolution rate, and mechanical properties, while preserving their pharmacological properties [3–6]. Moreover, the use of another drug component as a coformer may achieve the synergy of pharmaceutical efficacy with APIs.

Janus Kinase (JAK) is a family of intracellular non-receptor tyrosine kinases that mediate cytokine signaling. It is an essential pathway for immune response, but, on the

other hand, it may be over-activated during the development of inflammation, leading to the occurrence of diseases. JAK inhibitors have revolutionized the treatment of some heterogeneous diseases, such as rheumatoid arthritis, myeloproliferative neoplasms, and numerous inflammatory dermatological disorders [7–10]. SHR0302 ( $C_{18}H_{22}N_8O_2S$ , CAS No.: 1445987-21-2, Figure 1) is a new generation of JAK inhibitor, which has similar efficacy and safety to other JAK drugs in biologics, but it is cheaper and easier to use, and can significantly improve the treatment compliance of patients [11–13]. However, SHR0302 suffers the main disadvantage of poor solubility, only slightly soluble in dimethyl sulfoxide or 0.1mol/L sodium hydroxide, and nearly insoluble in anhydrous methanol, ethanol, or water. Therefore, the enhancement of its solubility property is desirable to improve the bioavailability and therapeutic efficacy [14–16].

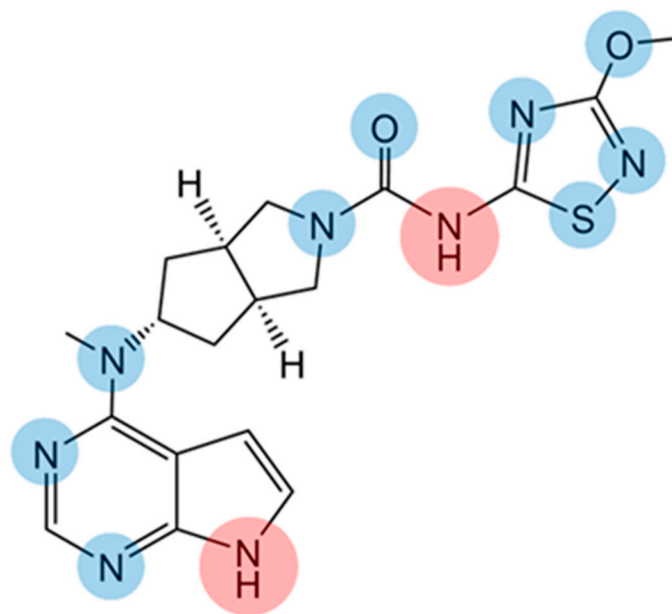


**Figure 1.** Chemical structure of SHR0302. Hydrogen bond receptors are highlighted in blue while hydrogen bond donors in red.

Generally speaking, the solubility and dissolution performance of APIs could be improved by either modification of chemical structure, e.g., forming inorganic salts with strong acid or base, or development of the aforementioned multicomponent crystal forms with organic coformers. The former may suffer chemical degradation and hygroscopicity issues because of the use of strong acids or bases. The multicomponent crystal form approach benefits from weak intermolecular interactions in essence and offers more opportunities in finely tuning pharmaceutical properties. The design, synthesis, and characterization of these solid forms are of vital importance to seeking the optimal physicochemical property of APIs [17]. However, the selection of appropriate coformers is time-consuming and experimentally costly, and the property optimization of multicomponent crystal forms of APIs relies on trial and error.

Various efforts on computational prediction and screening of coformers have been made to minimize the number of experimental trials, such as the conductor-like screening model for realistic solvents (COSMO-RS), molecular complementary (MC) analysis, Etter's rules [18], the  $\Delta pK_a$  rule [19], and Hansen solubility parameters [20]. Among these screening methods, the COSMO-RS approach [21,22] utilizes the binding affinity between APIs and coformer molecules, quantitatively assessed by the excess (or mixing) enthalpy ( $\Delta H_{ex}$ ), based upon the calculations of fundamental segment–segment electrostatic, hydrogen-bonding, and *van der Waals* interactions to rank and score the probability of coformers [23–25]. The MC screening method is based on molecular similarity analysis, characterized by indexes of molecule shape and polarity [26].

In this work, a total of 42 coformer candidates containing various functional groups and supramolecular synthons were selected from a coformer database aiming to capture as many multicomponent crystalline forms of SHR0302 as possible. To reduce the number of screening coformers, we established two screening strategies: COSMO-RS and MC, and their prediction performances and shortcomings were evaluated and discussed. Experimental screening via slurry crystallization and solvent-assisted grinding methods was conducted to synthesize new multicomponent crystal forms of SHR0302. The obtained multicomponent crystals were purified and characterized by powder X-ray diffraction, thermal analyses, and IR spectra. The proton transfer was analyzed and characterized by  $^1\text{H-NMR}$  spectroscopy. Further, the solubility performance of these multicomponent crystals was examined by equilibrium solubility measurement, showing an improved performance in comparison with API alone.

## 2. Theoretical Prediction Models

COSMO-RS, an effective tool based on quantum chemistry and statistical thermodynamics, is widely used for the prediction of thermodynamic equilibrium properties in liquid systems. In this approach, the distribution of polarization charge density  $\sigma$  on the molecular surface embedded in a virtual conductor (derived by the COSMO model) is reduced to a histogram, that is,  $\sigma$ -profile. It reflects how much of the surface segments could be found in a polarity interval. The  $\sigma$ -profile is defined by

$$P_i(\sigma) = \frac{n_i(\sigma)}{n_i} = \frac{A_i(\sigma)}{A_i} \quad (1)$$

where  $n_i$  is the total number of segments in a single molecule  $i$  with a total surface area  $A_i$ , and  $n_i(\sigma)$  is the number of segments with polarization charge density  $\sigma$  that have a surface area  $A_i(\sigma)$ . All charge density information is calculated through quantum mechanical calculation which can be obtained directly from COSMO output file.

Then, statistical thermodynamics is used to solve the ensemble of pairwise interacting surface segments, generating the  $\sigma$ -potential. In the COSMO-RS theory, the most important molecular interactions, such as electrostatic ( $E_{MF}$ ), hydrogen bonding ( $E_{HB}$ ), and *van der Waals* interaction ( $E_{vdW}$ ), are taken into account as functions of the polarization charges of two interacting surface segments  $\sigma$  and  $\sigma'$  ( $\sigma_{donor}$  and  $\sigma_{acceptor}$ ). The interactions are calculated by the follow equations:

$$E_{MF} = a_{eff} \frac{\alpha}{2} (\sigma + \sigma')^2 \quad (2)$$

$$E_{HB} = a_{eff} C_{HB} \min\{0, \min(0; \sigma_{donor} + \sigma_{HB}) \max(0; \sigma_{acceptor} - \sigma_{HB})\} \quad (3)$$

$$E_{vdW} = a_{eff} (\tau_{vdW} + \tau'_{vdW}) \quad (4)$$

where  $a_{eff}$  is the contact surface area;  $\alpha$  is an adjustable parameter (the energy factor); and  $C_{HB}$  and  $\sigma_{HB}$  are adjustable parameters of the HB interaction energy.  $\tau_{vdW}$  and  $\tau'_{vdW}$  are element-specific parameters of *van der Waals* interaction. As a result, the chemical potential of a surface segment with polarization charge density, i.e.,  $\sigma$ -potential  $\mu_s(\sigma)$ , is given by

$$\mu_s(\sigma) = -\frac{RT}{a_{eff}} \ln \left[ \int_s^p (\sigma') \exp \left\{ \frac{a_{eff}}{RT} (\mu_s(\sigma') - E_{MF}(\sigma, \sigma') - E_{HB}(\sigma, \sigma')) \right\} d\sigma' \right] \quad (5)$$

The  $\sigma$ -potential is integrated over the surface of a molecule, resulting in the chemical potential, based on which other thermodynamics data could be derived [27]. Among them, the excess enthalpy  $\Delta H_{ex}$  of a virtual supercooled liquid of the two-component mixture relative to the pure components is regarded as the parameter to evaluate the tendency of

those two molecules to form a cocrystal/salt [28]. The more negative the  $\Delta H_{ex}$  value is, the more likely it is for APIs to form a cocrystal/salt.

$$\Delta H_{ex} = H_{AB} - x_m H_{pure,A} - x_n H_{pure,B} \quad (6)$$

Here,  $H_{AB}$  and  $H_{pure}$  represent the molar enthalpy in  $m:n$  mixture and pure reference state, respectively, where molecular weight  $x_m = m/(m+n)$  and  $x_n = n/(m+n)$ . The excess enthalpies of APIs and coformers give a good estimate of the cocrystallization tendency, which can be derived from calculated enthalpies of each component ( $A$  and  $B$ ) and the mixture (a mixture of  $A$  and  $B$  of a given stoichiometric in subcooled liquid).

MC analysis is a structure-based method using the statistical correlation analysis of cocrystals in the Cambridge Structural Database (CSD). It proposes that molecules possessing similar geometrical shapes and polarities tend to co-crystallize together [29]. The similarities are assessed through the comparison of several geometric descriptors between two molecules. If two molecules prefer to crystallize together, the differences between the values of their descriptors should be small.

There are five descriptors selected to define the similarity, namely, the fraction of nitrogen and oxygen atoms, the dipole moment, and three simple shape descriptors based on a molecular bounding box—the length of the short axis, the short/long axis ratio, and the medium/long axis ratio (Figure S1). Each descriptor has a threshold to signal a “PASS” corresponding to the formation of a cocrystal while “FAIL” means no reaction. Overall, it predicts the formation of a cocrystal, if and only if, all five descriptors exhibit a “PASS” [30,31].

### 3. Experimental Section

#### 3.1. Materials

SHR0302 ( $\geq 99.0\%$ , GC) was received from Jiangsu Hengrui Pharmaceuticals Co., LTD. (Lianyungang, China). Salicylic acid, citric acid, 2,6-dihydroxybenzoic acid and 27 others (all greater than 99.0 wt%) were purchased from Aladdin Bio-Technology (Shanghai, China). The solvents (A.R.) such as isopropanol, acetonitrile, and dichloromethane were purchased from Jiangtian Chemical Technology (Tianjin, China). All chemicals were used without further purification.

#### 3.2. Preparation of Multicomponent Crystal Forms

Multicomponent crystal forms of SHR0302 were synthesized by the slurry crystallization method and/or solvent-assisted grinding method. In the slurry crystallization method, SHR0302 and coformers, at a fixed stoichiometric ratio (1:1), were added into the solvent. The mixture was stirred at room temperature for 24 h. Then, the suspension was filtered and dried at 40 °C for 3 h to obtain the products. In the solvent-assisted grinding method, SHR0302 and coformers, at a fixed stoichiometric ratio (1:1), were added into a ball mill with 50  $\mu$ L organic solvent in a stainless steel ball ( $\phi$  10 mm, 4 g) at 20 Hz for 30 min at room temperature, and then the samples were obtained. Experimental details of SHR0302-SAL, SHR0302-CA, and SHR0302-26DHBA are summarized in Table S1 and the others are basically identical.

#### 3.3. Virtual Coformer Screening

All the calculations of excess enthalpy between API and coformer were performed using the COSMOthermX\_3.0 program (COSMOlogic GmbH & Co. KG, Leverkusen, Germany). The COSMO files of a total of 42 coformers and the API used in this study were either taken directly from a database of DMol3-COSMO-PBE or generated using the DMol3 package from Accelrys at the DFT level, applying the functional of PBE and DNP basis sets [32,33]. Only stable conformations were taken into account in the calculations.

MC analysis of molecular similarity was carried out by the software Mercury 4.1.0. The default setting to use all five descriptors was applied. The coordination files of SHR0302 and coformers in .mol2 format were imported into Mercury for CSD analysis.

### 3.4. Powder X-ray Diffraction (PXRD)

Powder X-ray diffraction patterns were collected on a Rigaku D/MAX 2500 with Cu K $\alpha$  (1.54178 Å) radiation in the  $2\theta$  range of 2–40° at a scanning rate of 8° min<sup>−1</sup>. Data were collected at ambient temperature (25 °C). The tube voltage and current used were respectively 40 kV and 100 mA.

### 3.5. Thermal Analysis

Differential scanning calorimetry (DSC) was conducted with a Mettler DSC204. The samples weighing 3–5 mg were heated in pinhole pans at a scan rate of 10 °C min<sup>−1</sup> under a nitrogen gas flow of 50 mL min<sup>−1</sup>. The range of heating temperature was 25–200 °C.

Thermogravimetric analysis (TGA) was performed in the temperature range of 25–300 °C on a Mettler TGA/DSC 1 STAR<sup>e</sup> system, using a nitrogen gas purge flow of 20 mL min<sup>−1</sup> and a scan rate of 10 °C min<sup>−1</sup>.

### 3.6. Fourier-Transformed Infrared Spectrometer (FTIR)

IR spectra were collected on a Bruker FT-IR 750 infrared instrument (BRUKER, Karlsruhe, Germany). Each sample was scanned with the scan number of at least 32 over the spectral range 4000–400 cm<sup>−1</sup> at a resolution of 4 cm<sup>−1</sup>. Data were obtained at 25 °C.

### 3.7. NMR Spectroscopy

<sup>1</sup>H-NMR and two-dimensional (2D) NMR spectra were acquired on a 400 MHz Bruker Avance-III spectrometer at 298 K. Data were processed and analyzed using MestReNova software. NMR samples were prepared by dissolving a certain amount of three multicomponent crystals and the corresponding individual components in DMSO-d<sub>6</sub>. Chemical shifts ( $\delta$ ) were measured in units of parts per million (ppm).

### 3.8. Solubility Measurement

The equilibrium solubility data of three new multicomponent crystalline forms of SHR0302 were measured by suspending excess solid samples in DI water and 0.1 M HCl at 37.0 °C for at least 6 h. It is worth mentioning that the equilibrium temperature was chosen to simulate the in vivo condition. The clear supernatant was filtered by a 0.45  $\mu$ m nylon filter and diluted 30 times in aqueous solution. The solubility measurements were performed using high-performance liquid chromatography (HPLC, Waters 2695/2996). A chromatographic column (Waters Xselect-HSS-T3, 150  $\times$  4.6 mm, 3.5  $\mu$ m) was applied at 30.0 °C with the UV detection wavelength of 218 nm. The mobile phase of HPLC was potassium dihydrogen phosphate buffer (1.36g potassium dihydrogen phosphate, dissolved with 1000mL purified water, then 1ml triethylamine, adjusted pH to 2.8 with phosphoric acid) and acetonitrile (*v/v*:80/20), with a flow rate of 1.0 mL min<sup>−1</sup>.

## 4. Results and Discussion

### 4.1. Virtual Coformer Screening

A total of 42 cofomers covering a variety of functional groups and supramolecular synthons were selected (Figure 2), and their binding capabilities with the target JAK inhibitor drug, SHR0302, were examined for the development of new multicomponent crystal forms through calculations of COSMO-RS and MC. These cofomer molecules included carboxylic acid, hydroxyl, phenolic hydroxyl, and secondary amine functional groups (highlighted in red), which may function as hydrogen bonding donors due to the molecular structure of SHR0302 which is mostly rich in hydrogen bonding acceptor moieties including tertiary amines, carbonyl, and methyl ether. Some cofomers with either a hydrogen bonding acceptor, i.e., tertiary amine, or both a hydrogen bonding acceptor and donor were also selected (highlighted in blue). Since the possible polymorphism won't make a huge difference to the interaction between SHR0302 and cofomers, the discussion on this issue is not in the scope of this work.



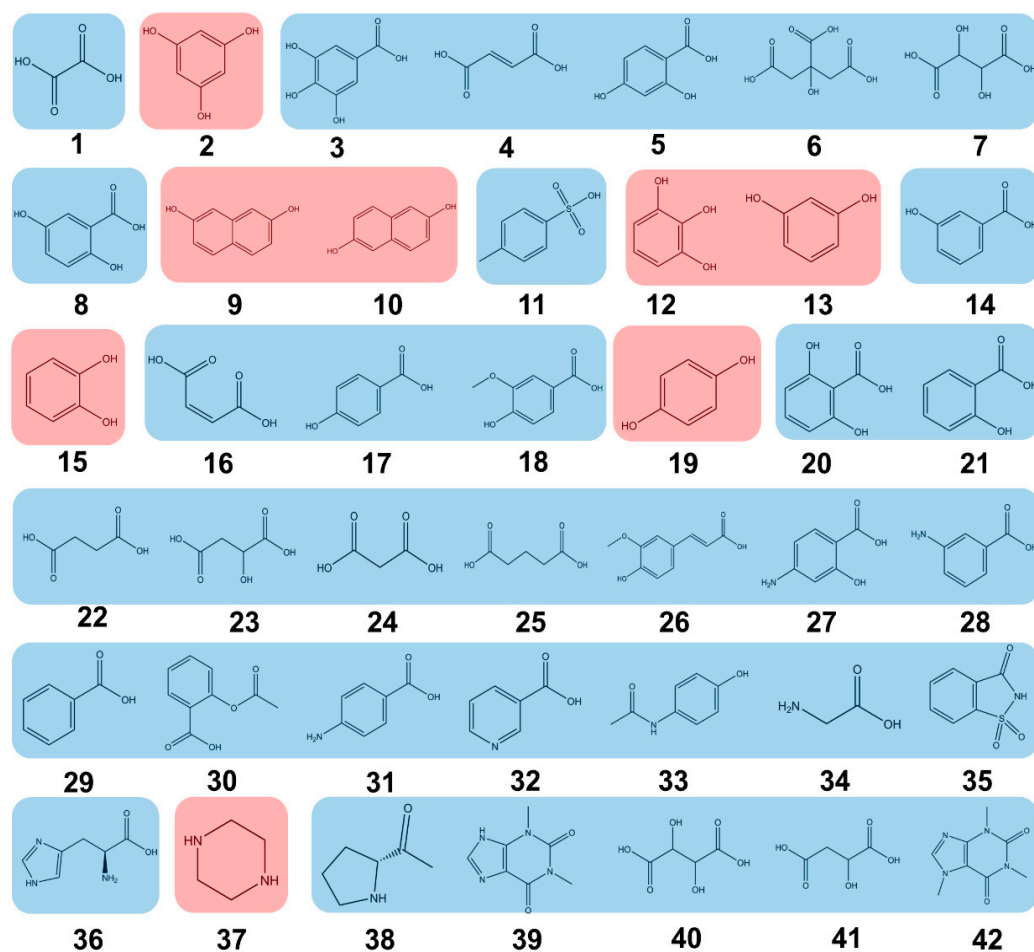


**Figure 2.** The selected 42 coformer database for synthesis of SHR0302 multicomponent crystal forms. The numbers in the figure represent 1 Oxalic Acid; 2 Phloroglucinol; 3 Gallic Acid; 4 Fumaric Acid; 5 2,4-Dihydroxybenzoic Acid; 6 Citric Acid; 7 Tartaric Acid; 8 2,5-Dihydroxybenzoic Acid; 9 2,7-Dihydroxynaphthalene; 10 2,6-Dihydroxynaphthalene; 11 *p*-Toluenesulfonic Acid; 12 Pyrogallol; 13 Resorcinol; 14 3-Hydroxybenzoic Acid; 15 Catechol; 16 Maleic Acid; 17 4-Hydroxybenzoic Acid; 18 Vanillic Acid; 19 Hydroquinone; 20 2,6-Dihydroxybenzoic Acid; 21 Salicylic Acid; 22 Succinic Acid; 23 L-Hydroxybutanedioic Acid; 24 Malonic Acid; 25 Glutaric Acid; 26 Ferulic Acid; 27 4-Aminosalicylic Acid; 28 *m*-Aminobenzoic Acid; 29 Benzoic Acid; 30 Acetylsalicylic Acid; 31 *p*-Aminobenzoic Acid; 32 Nicotinic Acid; 33 Acetaminophen; 34 Glycine; 35 Saccharin; 36 Histidine; 37 Piperazine; 38 Proline; 39 Theophylline; 40 Isoniazid; 41 Adipic Acid; and 42 Caffeine.

Figure 3 shows the list of predicted coformer structures ranked with the calculated values of excess enthalpy,  $\Delta H_{ex}$ , which is defined as the difference of molar enthalpies between a virtually supercooled liquid mixture and the corresponding pure components. The high value of excess enthalpy suggests strong interactions between API and coformer, and thereby the formation of cocrystal or salt is energetically favorable. The calculated  $\Delta H_{ex}$  values were found varying from +0.09 to  $-10.00 \text{ kcal}\cdot\text{mol}^{-1}$ . Further, coformers with carboxyl, hydroxyl, and phenolic hydroxyl moieties had more negative  $\Delta H_{ex}$  values, indicating a higher probability to form cocrystals from a theoretical perspective.

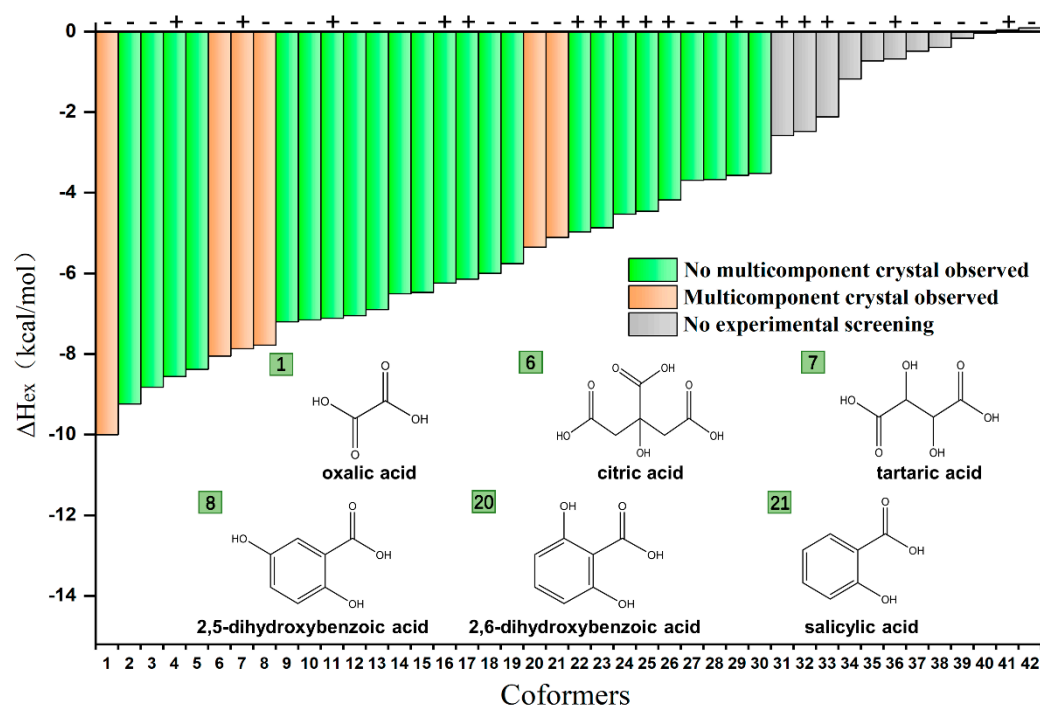


**Figure 3.** Virtual and experimental coformer screening results (the first 30 coformers) of SHR0302 multicomponent crystal forms ranked by  $\Delta H_{ex}$  values from COSMO-RS, along with prediction data from MC method.

Coformer predictions by MC method show that 16 out of 42 coformers were assessed to be able to form multicomponent crystals with SHR0302 (marked “+” in Figure 2). Since the MC analysis focused on the molecular similarity based on the index of molecule shape and polarity, these selected coformers are supposed to possess similar geometric descriptors compared to SHR0302, such as the fraction of nitrogen and oxygen atoms and the shape descriptors, and thus exhibited affinity with SHR0302.

Subsequently, we performed experimental screening from the reduced coformer database (the first 30 coformers) that had  $\Delta H_{ex}$  greater than  $-3.52$  kcal/mol. Experimental screening was performed using slurry crystallization and solvent-assisted grinding methods. Six new multicomponent crystal forms of SHR0302 were obtained with coformers of citric acid (CA), tartaric acid (TA), 2,5-dihydroxybenzoic acid (25DHBA), 2,6-dihydroxybenzoic acid (26DHBA), oxalic acid (OA), and salicylic acid (SAL). Interestingly, all coformers had at least one carboxyl functional group. Overall, COSMO-RS predicted successfully the strong binding affinity, as manifested by the low values of excess enthalpy (less than  $-5$  kcal mol $^{-1}$ ), between SHR0302 and coformers. Although some other coformers had comparable low values of excess enthalpy, they were not found forming multicomponent crystal forms with SHR0302, either because of deficiencies of COSMO-RS predictions or because it was not experimentally obtainable. However, it is worth mentioning that no hit does not mean that a multicomponent crystal form could not be obtained with other methods. By contrast, the MC approach performed worse with only one successful prediction (i.e., TA). It is worth mentioning that although six multicomponent crystal forms of SHR0302 were identified, we only performed detailed characterization and analyses on SHR0302-SAL, SHR0302-CA, and SHR0302-26DHBA crystalline phases accounting for the coformer’s toxicity and purification difficulty. Among them, salicylic acid can reduce inflammation, relieve pain, and treat fever. Citric acid can be used as an antioxidant, enhance appetite, and promote calcium and phosphorus absorption in the body. 2,6-dihydroxybenzoic acid is also an antioxidant. More detailed experimental screening results are shown in Table S2.

#### 4.2. Solid-State Characterization

##### 4.2.1. Power X-ray Diffraction (PXRD) Analysis

Figure 4 shows a comparison of PXRD patterns of three synthesized multicomponent crystals of SHR0302 with salicylic acid, citric acid, and 2,6-dihydroxybenzoic acid (SHR0302-SAL, SHR0302-CA, SHR0302-26DHBA) with the corresponding individual components. The newly formed PXRD peaks in the SHR0302-SAL sample at  $7.88^\circ$ ,  $14.90^\circ$ ,  $21.86^\circ$ , and  $23.92^\circ$  are distinct from those of SHR0302 and CA materials, indicating the formation of new multicomponent crystalline forms. Similarly, the SHR0302-CA formed new peaks at  $11.14^\circ$ ,  $19.02^\circ$ , and  $22.42^\circ$ , while SHR0302-26DHBA at  $8.36^\circ$ ,  $16.94^\circ$ ,  $17.79^\circ$ , and  $26.04^\circ$ , differing from the individual raw materials, which thereby indicate the formation of SHR0302-SAL and SHR0302-26DHBA multicomponent crystalline forms.

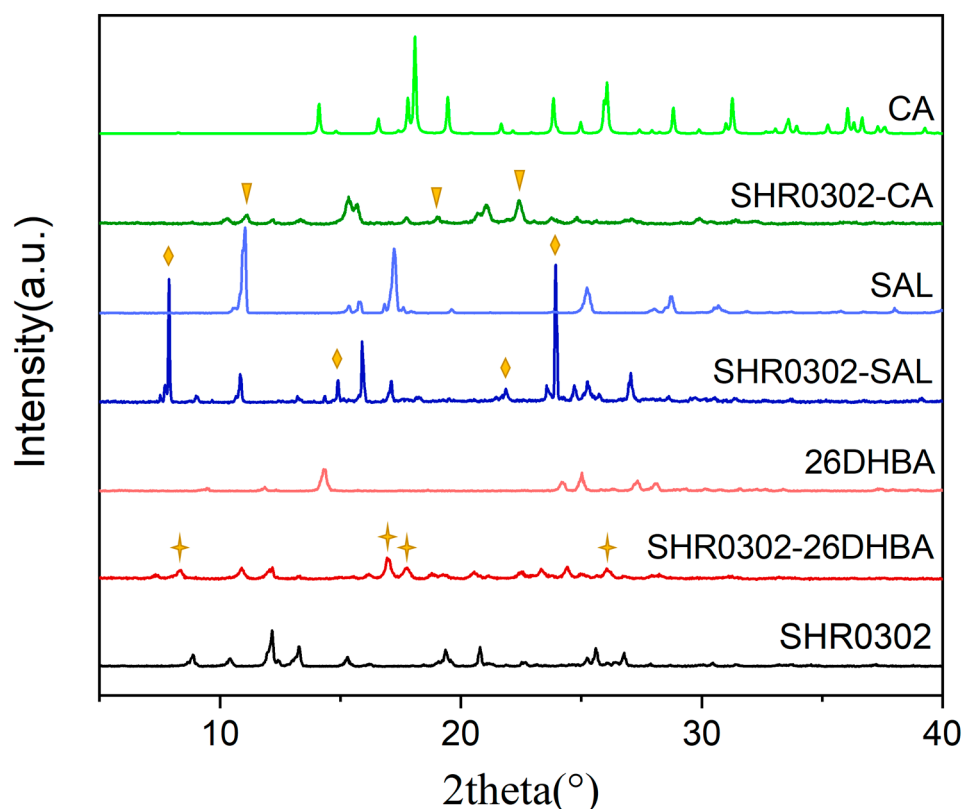


**Figure 4.** PXRD pattern comparisons of multicomponent crystalline forms of SHR0302-SAL, SHR0302-CA, and SHR0302-26DHBA, with the corresponding individual components. The triangle, diamond and star are used to point out the newly formed peaks.

##### 4.2.2. Thermal Analysis

Thermal analyses were performed to identify the phase purity and composition of crystalline samples. The DSC plots, along with TGA curves of SHR0302-SAL, SHR0302-CA, and SHR0302-26DHBA samples, are shown in Figure 5. It was found that the SHR0302-SAL sample displays only one sharp endothermic peak with onset point at  $180.1 \pm 1.0^\circ\text{C}$  prior to chemical degradation, differing from the melting point of raw material SHR0302 at  $259.6 \pm 1.0^\circ\text{C}$  and raw material SAL at  $158.8 \pm 1.0^\circ\text{C}$ , and thus can be unambiguously attributed to the melting of a new multicomponent crystalline phase. Similarly, the SHR0302-CA and SHR0302-26DHBA samples display only one characteristic melting peak at  $180.3 \pm 1.0^\circ\text{C}$  and at  $213.19 \pm 1^\circ\text{C}$ , respectively, which are distinct from either SHR0302 or cocrystals ( $155.7 \pm 1.0^\circ\text{C}$  for CA and  $164.8 \pm 1.0^\circ\text{C}$  for 26DHBA). Thereby, the results confirm the formation of multicomponent crystal forms of SHR0302-CA and SHR0302-26DHBA. Note that the melting of these multicomponent crystal forms accompanies chemical degradations (Figure S2).



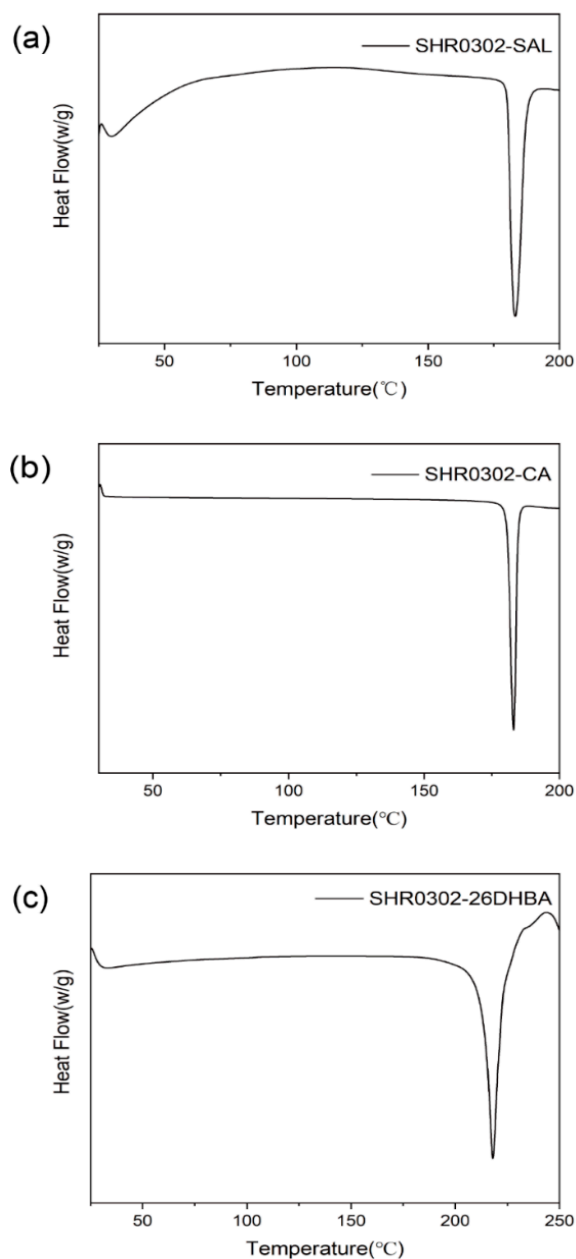


**Figure 5.** DSC plots of SHR0302-SAL (a), SHR0302-CA (b), and SHR0302-26DHBA (c) multicomponent crystal forms.

#### 4.2.3. FTIR Spectroscopy

FTIR spectroscopy was employed to further characterize the formation of SHR0302 multicomponent crystalline phases and to provide insights into their formation process. Figure 6 shows IR spectra of three multicomponent crystal forms of SHR0302 in comparison with individual raw materials. It was found that the characteristic IR peak of SHR0302 at  $1630\text{ cm}^{-1}$  disappears in the SHR0302-SAL spectrum, with the C-O vibration peak shifting from  $1262\text{ cm}^{-1}$  to  $1257\text{ cm}^{-1}$ . These changes support the formation of a new SHR0302-SAL phase (Figure 6a).

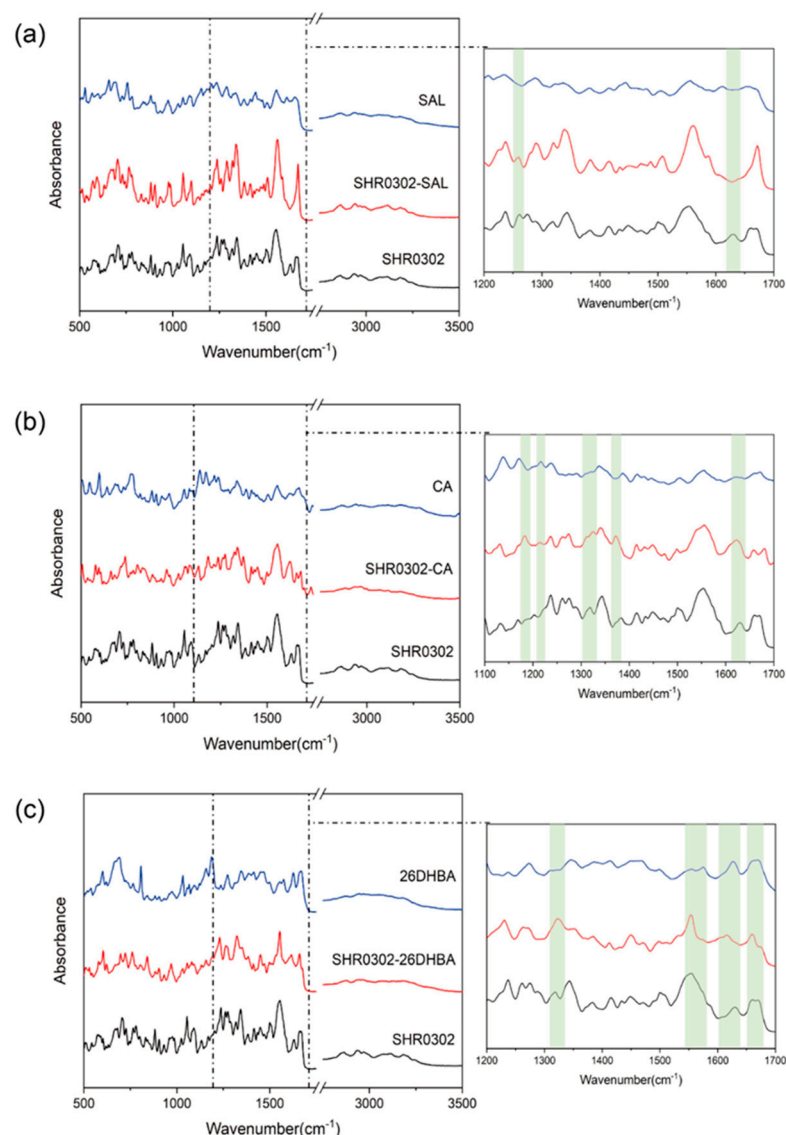


**Figure 6.** Comparisons of FTIR spectra of synthesized multicomponent crystal forms and the corresponding individual components for (a) SHR0302-SAL, (b) SHR0302-CA, and (c) SHR0302-26DHBA.

In the IR spectrum of SHR0302-CA (Figure 6b), the C-O vibration peak shifts from  $1216\text{ cm}^{-1}$  (SHR0302 sample) to  $1212\text{ cm}^{-1}$ , with the formation of a new characteristic carboxyl stretching vibration peak ( $1373\text{ cm}^{-1}$ ). The peak of C-N (secondary amine) of aromatic amine appears at  $1321\text{ cm}^{-1}$  in SHR0302, and shifts to  $1326\text{ cm}^{-1}$  in SHR0302-CA. Further, the N-H deformation vibration peak of SHR0302 observed at  $1629\text{ cm}^{-1}$  offsets to  $1624\text{ cm}^{-1}$  in SHR0302-CA. The stretching vibration peak of C=O in SHR0302-26DHBA shows a shift towards  $1662\text{ cm}^{-1}$  compared with SHR0302 (Figure 6c), which is associated with the intermolecular interactions between SHR0302 and 2, 6-dihydroxybenzoic acid. The peak of C-N (secondary amine) of aromatic amine at  $1317\text{ cm}^{-1}$  is observed in SHR0302 and shifts to  $1326\text{ cm}^{-1}$  in SHR0302-26DHBA. In addition, the conjugated C=N peak at  $1630\text{ cm}^{-1}$  in 2, 6-dihydroxybenzoic acid shifts to  $1616\text{ cm}^{-1}$  in the SHR0302-26DHBA sample. These distinct differences prove the formation of a new SHR0302-26DHBA crystalline phase. Further, we observed the disappearance of the stretching carbonyl (C=O) bands of 2, 6-dihydroxybenzoic acid ( $1574\text{ cm}^{-1}$  and  $1304\text{ cm}^{-1}$ ) in the SHR0302-26DHBA sample, which are reformed at  $1556\text{ cm}^{-1}$  and  $1326\text{ cm}^{-1}$ , indicating the carboxylate salt formation between SHR0302 and 2, 6-dihydroxybenzoic acid.

#### 4.2.4. $^1\text{H}$ -NMR Spectroscopy

$^1\text{H}$ -NMR spectroscopy was used to understand and identify proton transfer and intermolecular interactions between the API and coformers. Figure 7 shows the  $^1\text{H}$ -NMR spectra of SHR0302-SAL, SHR0302-CA, and SHR0302-26DHBA in  $\text{DMSO-d}_6$ . The molecular structure of SHR0302 displays two small peaks at 11.60 and 11.61 ppm in  $\text{DMSO-d}_6$ , corresponding to the amide and NH groups on the five-membered ring, respectively. The detailed proton assignments are given in Figure S3. These peaks, absent in salicylic acid solution, shift to 11.61 and 11.64 ppm in SHR0302-SAL solution. The downfield shift of the SHR0302 N-H proton is due to the reduction of the electron cloud density that weakens the shielding effect, suggesting the formation of hydrogen bonds between SHR0302 and salicylic acid. Given the minor changes in the pyrimidine ring proton chemical shift, for instance, less than 0.02 ppm, it is suggested that no proton transfer between API and coformer occurred. Therefore, the SHR0302-SAL multicomponent crystal form is likely in the form of cocrystals rather than a salt.

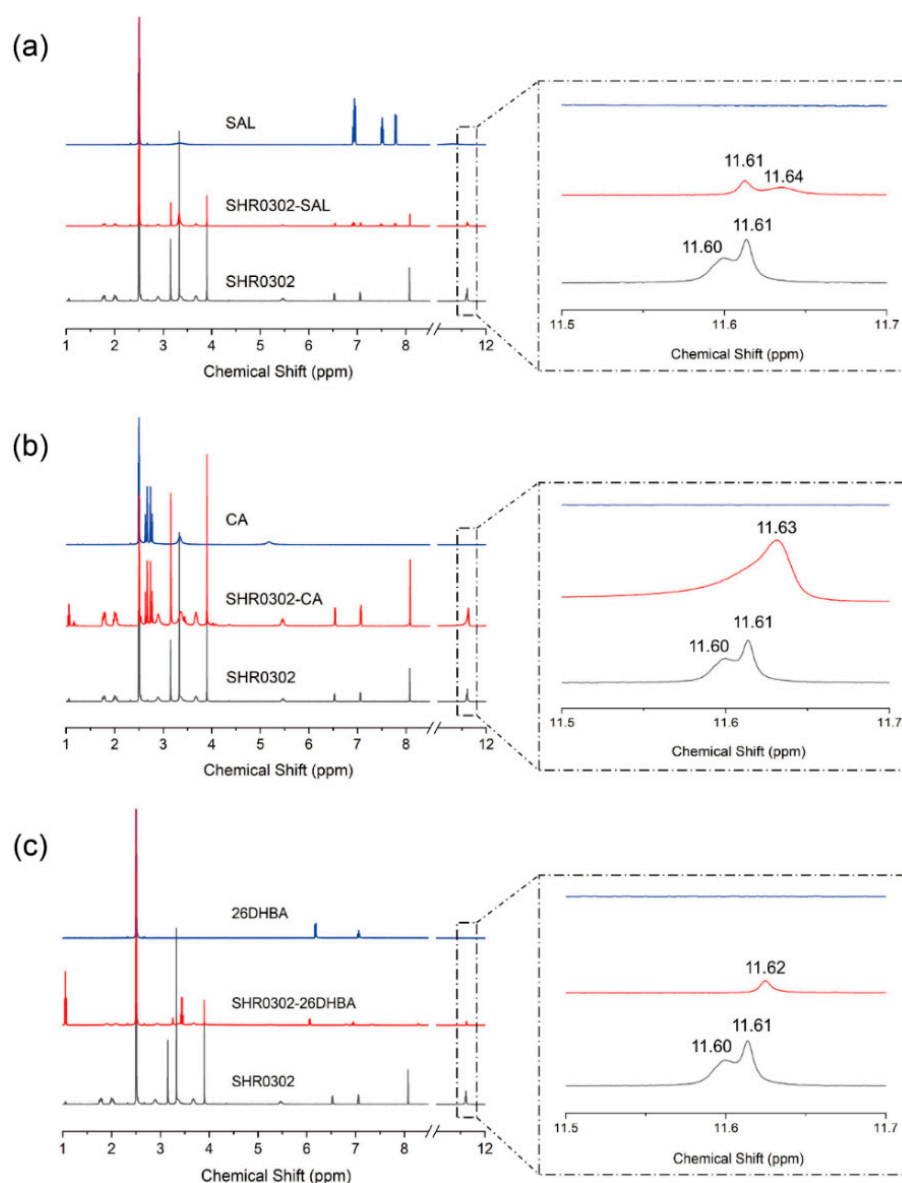


**Figure 7.**  $^1\text{H}$ -NMR spectra of (a) SHR0302-SAL, (b) SHR0302-CA, and (c) SHR0302-26DHBA, and the corresponding individual components.

The  $^1\text{H}$ -NMR spectrum of SHR0302-CA in  $\text{DMSO-d}_6$  only displays a broad peak at 11.63 ppm, with the amide proton disappearing, indicating that the carboxylic acid group of CA interacts with a SHR0302 nitrogen atom in the conjugate ring, and proton transfer occurs. The appearance of proton transfer increases the electron density of surrounding atoms and thus reduces the proton chemical shift. Indeed, we observed the proton resonance on the pyrrolo [2,3-d] pyrimidine ring of SHR0302 shifting to a high field. It is worth mentioning that the shoulder peak at 11.63 ppm may result from the presence of partially hydrogen bonding interactions. The results suggest that SHR0302 forms a salt with citric acid coformer. Similarly, the SHR0302-26DHBA sample also displays only a broad peak at 11.62 ppm, indicating interactions of the carboxylic acid group of 2,6-dihydroxybenzoic acid with a SHR0302 nitrogen atom on the conjugate ring and proton transfer. It is thus concluded that there is the formation of a salt between SHR0302 and 26DHBA.

#### 4.2.5. Intermolecular Interaction Analysis

In order to understand the fundamental interaction modes between SHR0302 and coformers, we computed their shielding charge density  $\sigma$ -profiles, shown in Figure 8. In COSMO-RS theory,  $\sigma$ -profile obtained from quantum chemical calculations is one of the most important molecule-specific properties. It is the distribution of the shielding charge density ( $\sigma$ ) of the molecule, which is divided into three regions including the nonpolar region ( $-0.0084 \text{ e}/\text{\AA}^2 < \sigma < 0.0084 \text{ e}/\text{\AA}^2$ ), the hydrogen bond donor region ( $\sigma < -0.0084 \text{ e}/\text{\AA}^2$ ), and the hydrogen bond acceptor region ( $\sigma > 0.0084 \text{ e}/\text{\AA}^2$ ) [28]. Moreover, the distribution of different regions can be visualized with the sigma surface. The red area on the sigma surface corresponds to the hydrogen bond donor region, while the blue area represents the hydrogen bond receptor region.

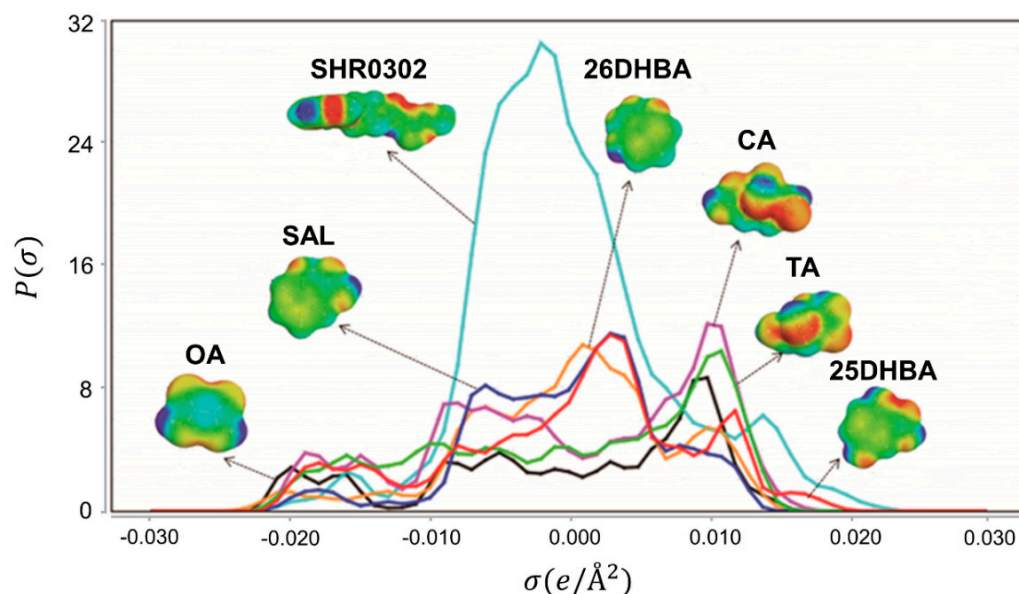


**Figure 8.**  $\sigma$ -profiles of SHR0302 and coformers. OA: oxalic acid; SAL: salicylic acid; 26DHBA: 2,6-dihydroxybenzoic acid; CA: citric acid; TA: tartaric acid; 25DHBA: 2,5-dihydroxybenzoic acid.

As seen from Figure 8, the  $\sigma$ -profile of SHR0302 is mainly distributed within the range of  $-0.02 \text{ e}/\text{\AA}^2 < \sigma < 0.02 \text{ e}/\text{\AA}^2$ , and has peaks in both the hydrogen bond donor region and hydrogen acceptor region. The peak of  $\sigma$ -profile located at the negative coordinate is due to the secondary amine in SHR0302, while the peak positioned at the positive coordinate is assigned to the O, N, and S atoms in SHR0302. Additionally, the  $\sigma$ -profiles of six selected coformers all possess peaks in the polar region, which makes them more likely to form hydrogen bonding interactions with SHR0302 and, consequently, generate new forms. The  $\sigma$ -profiles of coformers which cannot form new multicomponent crystal with SHR0302 are presented in Figure S4. Among them, catechol and pyrogallol act as pure hydrogen

bond donor, which possess no peak in the hydrogen acceptor region, and therefore have weaker interaction with SHR0302. Gallic acid and 2,4-dihydroxybenzoic acid have obvious peaks in the two polar regions indicating their high affinity with SHR0302, nonetheless, this inconsistency of computational prediction from experimental result may be associated with insufficient experimental search.

#### 4.3. Solubility Properties of SHR0302 Multicomponent Crystalline Forms

Previous studies have shown that the solubility of SHR0302 in water is around  $0.1 \text{ mg mL}^{-1}$  and is too low to be measured accurately in 0.1M HCl [34]. In order to evaluate the effect of multicomponent crystal forms on the solubility property, we measured the solubility of three synthesized multicomponent crystalline phases, and the results are shown in Table 1. It was found that the solubility of SHR0302 multicomponent crystal forms is significantly greater than the API alone in both water and 0.1 M HCl media (ca. less than  $0.1 \text{ mg mL}^{-1}$ ). The solubility in DI water increases up to threefold in SHR0302-CA salt form and up to twofold in SHR0302-SAL cocrystal form in comparison with the drug alone. Note that SHR0302-26DHBA is the exceptional one, for its solubility is  $0.02 \text{ mg/mL}$  in water, the lowest among all the synthesized crystals. This may be due to the hydrogen bonding structure of SHR0302-26DHBA cocrystals decreasing the polarity of the molecular complex and increasing the hydrophobic property. It is noted that the solubility of the three multicomponent crystalline phases in 0.1 M HCl is significantly higher than in water, which may be associated with the acidity of coformers. Overall, the solubility of SHR0302 has been demonstrated to be improved by developing multicomponent crystals [24,25].

**Table 1.** Solubility (mg/mL) of SHR0302 and Multicomponent Crystals in Water and 0.1 M HCl.

	Water	0.1 M HCl
SHR0302	0.10	\
SHR0302-SAL	0.17	1.56
SHR0302-CA	0.33	1.30
SHR0302-26DHBA	0.02	0.41

#### 4.4. Evaluation of COSMO-RS Prediction Performance

Prediction performance of the COSMO-RS model for synthesis of multicomponent crystal forms was evaluated by receiver operator characteristic (ROC) curve, presented in Figure 9. A ROC curve plots a true positive prediction rate (TPR) versus a false positive prediction rate (FPR) for a binary classifier system as its discrimination threshold ( $\Delta H_{ex}$  cutoff) is varied from small to higher values. Moreover, the area under the curve (AUC, denoted as A) quantitatively measures the performance of the ROC curve, which means that predictions with a higher value of AUC are generally better. The AUC of a useful prediction model should always be higher than 0.5, which indicates that it is superior to random selection, and the value of 1.0 corresponds to perfect prediction.

The performance of coformers screening based on the  $\Delta H_{ex}$  as computed with the COSMOthermX performed well with an AUC value of 0.81, significantly higher than that of random prediction, 0.5. In other words, the establishment of this model can effectively shorten the screening process compared with random experimental trials. An appropriate discrimination threshold ( $\Delta H_{ex}$  cutoff), which is supposed to achieve higher TPR and lower FPR, is needed as a guideline in the search for the coformers when the validity of the model has been confirmed. The Youden index, a commonly used statistical measure for prediction effectiveness, can balance TPR and FPR to obtain an optimal threshold. The Youden index is numerically equal to the difference between TPR and FPR. Thus, a threshold with the highest Youden index would be an optimal value corresponding to a high TPR with a low FPR. In this work, the highest Youden index is 0.58 when the  $\Delta H_{ex}$  cutoff was chosen as  $-5.11 \text{ kcal/mol}$  (Table S3). When such a threshold was applied, the number of experimental trials for SHR0302 multicomponent crystal forms could be



reduced to within 20 trials, only half the space of selected coformers. It is noted that the calculation of TPR and FPR depends on the prediction results of the COSMO-RS model and the results of experimental screening, indicating the accuracy of experimental data will impact significantly the result of the evaluation.

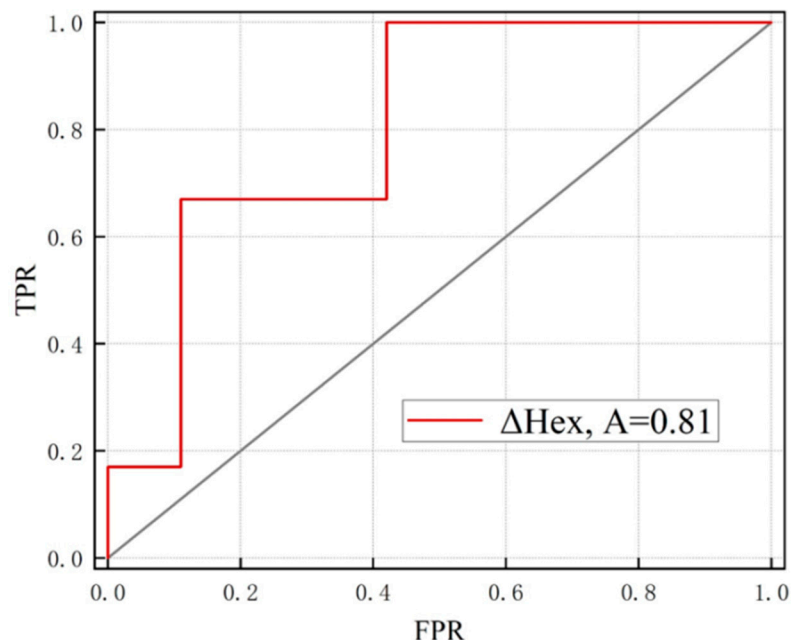


**Figure 9.** Receiver operator characteristic (ROC) curves measure the prediction performance of multicomponent crystalline forms based on  $\Delta H_{ex}$  values in COSMO-RS.

## 5. Conclusions

In this study we present a combined computational and experimental screening on the development of multicomponent crystal forms of a new class of Janus Kinase (JAK) inhibitor drug, SHR0302, with improved solubility performance. A total of 42 selected coformers were examined, and this large coformer screening space could be significantly reduced by COSMO-RS prediction of binding affinity between the API and coformers. Six new multicomponent crystal forms of SHR0302 were experimentally obtained with three of the coformers. These were SHR0302-salicylic acid cocrystal, SHR0302-citric acid salt, and SHR0302-2,6-dihydroxybenzoic acid salt, fully characterized by powder X-ray diffraction, thermal analyses, and IR and  $^1\text{H}$ -NMR spectroscopy. The proton transfer was confirmed between SHR0302 and coformers in SHR0302-citric acid and SHR0302-2,6-dihydroxybenzoic acid multicomponent crystals. Further, the equilibrium solubility measurement revealed the remarkable improvement in solubility in two of the newly synthesized multicomponent crystals in comparison with the drug alone. To assess the effectiveness of the COSMO-RS model, a receiver operator characteristic (ROC) curve was used. From the ROC curve, the area under the curve (AUC) was obtained which revealed that the model can significantly shorten screening time, and a conformable threshold was confirmed through the calculation of the Youden index. Together, this work demonstrated the improved solubility performance of SHR0302 by the development of multicomponent crystals and verified the reliability of the COSMO-RS method in coformer screening.

**Supplementary Materials:** The following supporting information can be downloaded at: <https://www.mdpi.com/article/10.3390/cryst12121722/s1>, Table S1: experimental details for preparation of multicomponent crystals; Tables S2 and S3: computation predictions of coformers and prediction performance evaluation; Figure S1: molecular bounding box model with three unequal dimensions; Figures S2 and S3: TGA data and predicted  $^1\text{H}$ -NMR spectra with proton assignments; Figure S4:  $\sigma$ -profiles of SHR0302 and coformers which cannot form new multicomponent crystal with SHR0302.

**Author Contributions:** Conceptualization, W.T. and W.G.; methodology, G.S., S.L. and Y.X.; software, G.S. and Y.X.; validation, G.S., S.L. and Y.X.; formal analysis, G.S. and W.T.; investigation, Y.X. and G.S.; resources, W.G., Y.H., C.Z. and J.G.; data curation, Y.X.; writing—original draft preparation, Y.X. and W.T.; writing—review and editing, Y.X., W.T., J.S. and W.G.; visualization, Y.X. and W.T.; supervision, W.T. and J.G.; project administration, W.T., W.G., Y.H., C.Z. and J.G.; funding acquisition, W.T., Y.H., C.Z., W.G. and J.G. All authors have read and agreed to the published version of the manuscript.

**Funding:** This research and the APC was funded by National Natural Science Foundation of China grant numbers NNSFC 22278300 and 21808159 and Natural Science Foundation of Tianjin grant number 19JCQNJC04800.

**Institutional Review Board Statement:** Not Applicable.

**Informed Consent Statement:** Not Applicable.

**Data Availability Statement:** Not Applicable.

**Acknowledgments:** The authors are grateful for the financial support of the National Natural Science Foundation of China (NNSFC 22278300 and 21808159) and the Natural Science Foundation of Tianjin (19JCQNJC04800).

**Conflicts of Interest:** The authors declare no conflict of interest.

## References

- Thakuria, R.; Delori, A.; Jones, W.; Lipert, M.P.; Roy, L.; Rodríguez-Hornedo, N. Pharmaceutical cocrystals and poorly soluble drugs. *Int. J. Pharm.* **2013**, *453*, 101–125. [\[CrossRef\]](#)
- Blagden, N.; de Matas, M.; Gavan, P.T.; York, P. Crystal engineering of active pharmaceutical ingredients to improve solubility and dissolution rates. *Adv. Drug Deliv. Rev.* **2007**, *59*, 617–630. [\[CrossRef\]](#)
- Rajput, L.; Sanphui, P.; Desiraju, G.R. New solid forms of the anti-HIV drug etravirine: Salts, cocrystals, and solubility. *Cryst. Growth Des.* **2013**, *13*, 3681–3690. [\[CrossRef\]](#)
- Kaplinksky, E. Sacubitril/valsartan in heart failure: Latest evidence and place in therapy. *Ther. Adv. Chronic Dis.* **2016**, *7*, 278–290. [\[CrossRef\]](#)
- Zhang, Y.; Du, X.; Wang, H.; He, Z.; Liu, H. Sacubitril-valsartan cocrystal revisited: Role of polymer excipients in the formulation. *Expert Opin. Drug Deliv.* **2021**, *18*, 515–526. [\[CrossRef\]](#)
- Almansa, C.; Merce, R.; Tesson, N.; Farran, J.; Tomas, J.; Plata-Salaman, C.R. Co-Crystal of Tramadol hydrochloride–Celecoxib (CTC): A novel API-API co-crystal for the treatment of pain. *Cryst. Growth Des.* **2017**, *17*, 1884–1892. [\[CrossRef\]](#)
- Rawlings, J.S.; Rosler, K.M.; Harrison, D.A. The JAK/STAT signaling pathway. *J. Cell Sci.* **2004**, *117*, 1281–1283. [\[CrossRef\]](#)
- Liongue, C.; Sertori, R.; Ward, A.C. Evolution of cytokine receptor signaling. *J. Immunol.* **2016**, *197*, 11–18. [\[CrossRef\]](#)
- Stark, G.R.; Darnell, J.E., Jr. The JAK-STAT pathway at twenty. *Immunity* **2012**, *36*, 503–514. [\[CrossRef\]](#)
- McLornan, D.P.; Pope, J.E.; Gotlib, J.; Harrison, C.N. Current and future status of JAK inhibitors. *Lancet* **2021**, *398*, 803–816. [\[CrossRef\]](#)
- Wu, H.; Yan, S.; Chen, J.; Luo, X.; Li, P.; Jia, X.; Dai, X.; Wang, C.; Huang, Q.; Liu, L.; et al. JAK1-STAT3 blockade by JAK inhibitor SHR0302 attenuates inflammatory responses of adjuvant-induced arthritis rats and decreases Th17 and total B cells. *Jt. Bone Spine* **2016**, *83*, 525–532. [\[CrossRef\]](#) [\[PubMed\]](#)
- Zhao, Y.; Zhang, L.; Ding, Y.; Tao, X.; Ji, C.; Dong, X.; Lu, J.; Wu, L.; Wang, R.; Lu, Q.; et al. Efficacy and Safety of SHR0302, a Highly Selective Janus Kinase 1 Inhibitor, in Patients with Moderate to Severe Atopic Dermatitis: A Phase II Randomized Clinical Trial. *Am. J. Clin. Dermatol.* **2021**, *22*, 877–889. [\[CrossRef\]](#) [\[PubMed\]](#)
- Sun, X.; He, Q.; Yang, J.; Wang, A.; Zhang, F.; Qiu, H.; Zhou, K.; Wang, P.; Ding, X.; Yuan, X.; et al. Preventive and Therapeutic Effects of a Novel JAK Inhibitor SHR0302 in Acute Graft-Versus-Host Disease. *Cell Transplant.* **2021**, *30*, 9636897211033778. [\[CrossRef\]](#) [\[PubMed\]](#)
- Di, L.; Kerns, E. *Drug-Like Properties: Concepts, Structure Design and Methods from ADME to Toxicity Optimization*; Academic Press: San Diego, CA, USA, 2008; pp. 61–92.
- Marques, M.R.; Choo, Q.; Ashtikar, M.; Rocha, T.C.; Bremer-Hoffmann, S.; Wacker, M.G. Nanomedicines-tiny particles and big challenges. *Adv. Drug Deliv. Rev.* **2019**, *151*, 23–43. [\[CrossRef\]](#) [\[PubMed\]](#)
- Fernández Casares, A.; Nap, W.M.; Ten Figás, G.; Huizenga, P.; Groot, R.; Hoffmann, M. An evaluation of salt screening methodologies. *J. Pharm. Pharmacol.* **2015**, *67*, 812–822. [\[CrossRef\]](#) [\[PubMed\]](#)
- Zhao, Y.; Sun, B.; Jia, L.; Wang, Y.; Wang, M.; Yang, H.; Qiao, Y.; Gong, J.; Tang, W. Tuning physicochemical properties of antipsychotic drug aripiprazole with multicomponent crystal strategy based on structure and property relationship. *Cryst. Growth Des.* **2020**, *20*, 3747–3761. [\[CrossRef\]](#)
- Etter, M.C. Hydrogen bonds as design elements in organic chemistry. *J. Phys. Chem.* **1991**, *95*, 4601–4610. [\[CrossRef\]](#)
- Cruz-Cabeza, A.J. Acid–base crystalline complexes and the pK<sub>a</sub> rule. *CrystEngComm* **2012**, *14*, 6362–6365. [\[CrossRef\]](#)

20. Mohammad, M.A.; Alhalaweh, A.; Velaga, S.P. Hansen solubility parameter as a tool to predict cocrystal formation. *Int. J. Pharm.* **2011**, *407*, 63–71. [[CrossRef](#)]
21. Klamt, A. The COSMO and COSMO-RS solvation models. *WIREs. Comput. Mol. Sci.* **2011**, *1*, 699–709. [[CrossRef](#)]
22. Loschen, C.; Klamt, A. Computational screening of drug solvates. *Pharm. Res.* **2016**, *33*, 2794–2804. [[CrossRef](#)]
23. Abramov, Y.A.; Loschen, C.; Klamt, A. Rational coformer or solvent selection for pharmaceutical cocrystallization or desolvation. *J. Pharm. Sci.* **2012**, *101*, 3687–3697. [[CrossRef](#)] [[PubMed](#)]
24. Wu, D.; Li, J.; Xiao, Y.; Ji, X.; Li, C.; Zhang, B.; Hou, B.; Zhou, L.; Xie, C.; Gong, J.; et al. New salts and cocrystals of pymetrozine with improvements on solubility and humidity stability: Experimental and theoretical study. *Cryst. Growth Des.* **2021**, *21*, 2371–2388. [[CrossRef](#)]
25. Lin, B.; Liu, Y.; Wang, M.; Wang, Y.; Du, S.; Gong, J.; Wu, S. Intermolecular interactions and solubility behavior of multicomponent crystal forms of orotic acid: Prediction and experiments. *Cryst. Growth Des.* **2021**, *21*, 1473–1481. [[CrossRef](#)]
26. Fábíán, L. Cambridge structural database analysis of molecular complementarity in cocrystals. *Cryst. Growth Des.* **2009**, *9*, 1436–1443. [[CrossRef](#)]
27. Loschen, C.; Klamt, A. Solubility prediction, solvate and cocrystal screening as tools for rational crystal engineering. *J. Pharm. Pharmacol.* **2015**, *67*, 803–811. [[CrossRef](#)]
28. Eckert, F.; Klamt, A. Fast solvent screening via quantum chemistry: COSMO-RS approach. *AIChE J.* **2002**, *48*, 369–385. [[CrossRef](#)]
29. Sarkar, N.; Gonnella, N.C.; Krawiec, M.; Xin, D.; Aakeröy, C.B. Evaluating the predictive abilities of protocols based on hydrogen-bond propensity, molecular complementarity, and hydrogen-bond energy for cocrystal screening. *Cryst. Growth Des.* **2020**, *20*, 7320–7327. [[CrossRef](#)]
30. Groom, C.R.; Bruno, I.J.; Lightfoot, M.P.; Ward, S.C. The Cambridge Structural Database. *Acta Crystallogr. Sect. B Struct. Sci. Cryst. Eng. Mater.* **2016**, *72*, 171–179. [[CrossRef](#)]
31. Pallipurath, A.R.; Civati, F.; Eziashi, M.; Omar, E.; McArdle, P.; Erxleben, A. Tailoring Cocrystal and Salt Formation and Controlling the Crystal Habit of Diflunisal. *Cryst. Growth Des.* **2016**, *16*, 6468–6478. [[CrossRef](#)]
32. Clark, S.J.; Segall, M.D.; Pickard, C.J.; Hasnip, P.J.; Probert, M.I.; Refson, K.; Payne, M.C. First principles methods using CASTEP. *Z. Krist. Cryst. Mater.* **2005**, *220*, 567–570. [[CrossRef](#)]
33. Perdew, J.P.; Burke, K.; Ernzerhof, M. Generalized gradient approximation made simple. *Phys. Rev. Lett.* **1996**, *77*, 3865. [[CrossRef](#)] [[PubMed](#)]
34. Sun, P.; Wu, G.; Gao, X.; Shen, L. A Bisulfate of JAK Kinase Inhibitor and Its Preparation Method. CN104470927B, 4 May 2016.